

A wettability switchable surface by microscale surface morphology change

This article has been downloaded from IOPscience. Please scroll down to see the full text article.

2007 J. Micromech. Microeng. 17 489

(<http://iopscience.iop.org/0960-1317/17/3/010>)

View [the table of contents for this issue](#), or go to the [journal homepage](#) for more

Download details:

IP Address: 144.214.80.138

The article was downloaded on 08/10/2012 at 07:15

Please note that [terms and conditions apply](#).

A wettability switchable surface by microscale surface morphology change

Ting-Hsuan Chen¹, Yun-Ju Chuang², Ching-Chang Chieng^{1,2}
and Fan-Gang Tseng^{1,2,3}

¹ Institute of Microelectromechanical System, National Tsing Hua University, 101, Sec. 2, Kuang-Fu Rd, Hsinchu 30013, Taiwan, Republic of China

² Department of Engineering and System Science, National Tsing Hua University, 101, Sec. 2, Kuang-Fu Rd, Hsinchu 30013, Taiwan, Republic of China

³ Research Center for Applied Sciences, Academia Sinica, 128, Sec. 2, Academia Rd, Nankang, Taipei 115, Taiwan, Republic of China

E-mail: fangang@ess.nthu.edu.tw

Received 17 August 2006, in final form 6 January 2007

Published 6 February 2007

Online at stacks.iop.org/JMM/17/489

Abstract

A novel wettability switchable surface which shields out any interference from driving energy is demonstrated. In this mechanism, a free-standing metal/polymer membrane with hydrophobic microposts is sustained by spacers, and electrostatic force is used to carry out the deflection of the metal/polymer membrane, hence changing the surface morphology as well as the fraction of a liquid/solid interface. Water contact angles under this mechanism can be manipulated from 131° to 152°, depending on the fraction of a liquid/solid interface. Since the driving energy of electrostatic action is shielded out by the ground electrode, the ingredients carried in the droplet can be thoroughly free from the interference and maintain functionality. Therefore, this mechanism has great potential to manipulate microdroplets for digital fluidic systems in bio-applications.

(Some figures in this article are in colour only in the electronic version)

1. Introduction

Wettability is an important property depending on the surface free energy and surface roughness. Recently, wettability control has attracted extensive interests for the development of smart devices, such as self-clean surfaces [1], discrete liquid droplet manipulators [2] or tunable optical lenses [3]. Due to the correlation with a surface tension gradient, a more dominant force in micro/nanoscale, wettability control provides a more flexible and efficient way for versatile applications. There have been many methods reported for reversible wettability switching, including thermocapillary [4], thermal chemistry [5], electrostatic molecule bending [6], electrowetting [7–9], light-induced surface chemistry [10], electrochemistry [11, 12] and mechanical surface morphology change [13]. The thermocapillary method utilizes the phenomenon that liquid contact angles change under different surface temperatures to control wettability reversibly [4]. It is an effective way to alternate surface wettability, but thermal energy cannot be prevented from affecting bio-molecules

inside droplets, and thermal energy would accelerate aqueous droplet evaporation as well. On the other hand, the thermal chemistry method employs a very low temperature difference, usually smaller than 20 °C, to induce molecule structure transformation between straight or tangled chain formations [5]. Such a molecular formation change enables the hydrophobic or hydrophilic part of the molecular chain to become exposed to a liquid droplet; hence, the wettability is changed. However, the switch efficacy might be affected by environment temperature, and the response is very slow (about tens of minutes). Electrostatic or electrowetting actuation employs electrostatic force to either bend down surface molecules [6] or provide charging attraction force to lower down the contact angle for wettability switch [7–9]. However, electrostatic energy can unavoidably penetrate into a droplet and pose carried bio-molecules adsorption on surface which may also fail the switching mechanism [14]. In addition, electrolysis would occur at the pinholes of the insulator. In the method of light-induced surface chemistry for droplet manipulation, high energy lights, such as ultraviolet (UV)

light [10], are required to change the structures of surface molecules from hydrophobic to hydrophilic. Nevertheless, the high-energy light may have the possibility of breaking the chains/bonds of bio-molecules carried by droplet, and the response is usually inefficient (about tens of seconds). Despite the fact that the response under UV light could be more rapid while the wavelength is correctly chosen, it is still unsuitable for the bio-application. From the methods mentioned above, the applied energies, such as thermal, electrical or UV light, for wettability manipulation are usually accompanied by a certain interference with bio-molecules carried by droplets and pose either bio-compatibility or switching functionality problems [14]. In contrast, electrochemistry provides another way to reversibly change the surface wettability by electrochemical doping and dedoping. In this method, the driving voltage for surface wettability switching is relatively small, so the interference from the electrical field could be neglected. Nevertheless, the required electrolytic environment and complex procedure for the switching mechanism are inconvenient for practical applications [11, 12].

On the other hand, surface roughness is an alternative way to manipulate surface wettability [15]. In order to enhance the effectiveness of electrowetting, a concept to combine the effect of electrowetting and surface roughness is investigated [16]. However, the reversible wettability change is limited by surface hysteresis. Another work reported to reversibly switch surface roughness is by bending the sustained poly(dimethylsiloxane) (PDMS) membrane through air pump suction [13]. Although such pressure-driven actuation is able to avoid the interference with droplet, the actuation is global and difficult to localise in a large array format. Thus, according to the limitation of literature, this paper aimed at developing a novel way to achieve wettability switching by employing shielded electrostatic energy for surface morphology change. In contrast with other works, this method encompasses abilities including changing the surface wettability without interference with the droplet, localizing the actuation in a large array and responding to the actuation rapidly.

2. Design

The design concept of the SWIM (surface wetting induced by morphology change) mechanism is shown in figure 1. A conductive metal/polymer composite membrane, supporting hydrophobic microposts of various heights, is sustained by negative photoresist spacers. Before applying an electric potential (initial state), a droplet is bolstered on the higher microposts [17], as shown in figure 1(a). As an electrical potential is applied between the conductive polymer membrane and the bottom addressable electrodes (actuated state), the membrane is bent due to the electrostatic force and the higher microposts will be lowered down. In order to achieve the minimum value of the surface free energy, the droplet will attach to the lower posts and the contact angle will decrease resulting from the increase of the contact interface between the droplet and the surfaces of the posts, as shown in figure 1(b). Accordingly, after switching off the electrical potential, the droplet will detach from the lower posts and merely contact with the higher posts due to the recovery of the membrane, thus switching back to the original contact

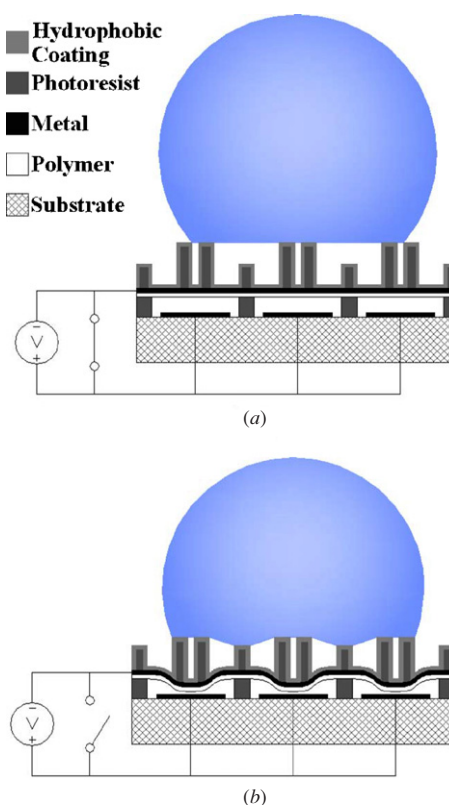


Figure 1. The operation concept of SWIM: (a) at initial state, the droplet merely contacts with the higher posts and (b) at actuated state, the droplet will contact with both the higher and lower posts. Hence, it is workable to reversibly switch the surface wettability by changing the contact area of the liquid/solid interface.

angle. Hence, we can locally and reversibly switch the surface wettability by changing the contact area of a liquid/solid interface without a sluggish response. Furthermore, since the electric field for membrane actuation is confined between the top conductive membrane (set to ground) and the bottom electrode, the electrical field would not penetrate into the droplet because of the shielding effect from the top grounded membrane. Therefore, the proposed method is more suitable to many applications, especially biological ones, because of the elimination of interference in the droplet.

3. Theory

The operation concept can be further explained by the prediction of Gibbs free energy (surface free energy) [18] and Cassie theory [17]. Gibbs free energy is one of the most important thermodynamic properties for characterizing a system. Besides, it is also the factor determining the final state of a system since the elements in the system always follow the rule to minimize the total amount of Gibbs free energy. This trend is described as equation (1):

$$\Delta G = \gamma \times \Delta A \leq 0. \quad (1)$$

ΔG means the variation of Gibbs free energy between different system states, where A is the interface area and γ is the free energy coefficient. As discussed above, since the system

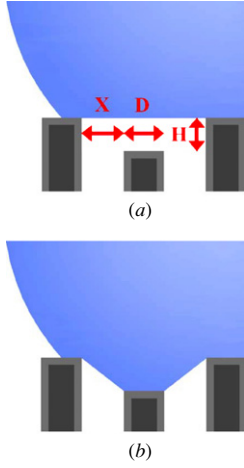


Figure 2. The probable mode at each state for further theory explanation: (a) detached mode: droplet detach from the lower posts and (b) attached mode: droplet attach to the lower posts.

always progresses toward the state where the total Gibbs free energy is minimal, ΔG must be a negative value under this trend.

Generally, the contact angle of a water droplet has been commonly used as a criterion for the evaluation of surface wettability. Based on Young's equation [18], the contact formation of the droplet on a smooth surface is determined by the minimum value of Gibbs free energy, expressed by equation (2):

$$\cos \theta = \frac{(\gamma_{sg} - \gamma_{sl})}{\gamma_{lg}}, \quad (2)$$

where γ_{sl} , γ_{sg} and γ_{lg} are the interfacial free energy coefficients of the liquid/solid, solid/gas and liquid/gas interfaces, and θ is the final contact angle. Comparing with equation (1), Young's equation is based on the requirement of a minimum energy state on a smooth and flat surface. In case the droplet contacts with a rough and hydrophobic surface, Young's equation needs additional modification. The Cassie theory [17] described that a droplet is bolstered by the upper part of the roughness surface, so the projected area of the droplet is composed of a liquid/solid interface and liquid/gas interface. The relationship between the contact angle and the area fraction of the liquid/solid surface is shown as follows:

$$\begin{aligned} \cos \theta' &= f \cos \theta + (1 - f) \cos 180^\circ \\ &= f \cos \theta + f - 1, \end{aligned} \quad (3)$$

where $f = A_{sl}/(A_{sl} + A_{gl})$ represents the area fraction of the liquid/solid interface, and θ as well as θ' denote the contact angles on a smooth and rough surface, respectively. Thus, the contact angle will increase with the decrease of the contact area of the liquid/solid interface and vice versa.

To verify the reversibility of the liquid/solid interface change, we defined two modes: the detached mode (droplet detaches from the lower posts) and the attached mode (droplet attaches to the lower posts), as shown in figures 2(a) and (b). These two modes represent the probable droplet mode at either initial state or actuated state. Following the surface free energy definition (equation (1)), in two dimensions, the surface free energies G_d and G_a at the detached mode and attached modes are described as

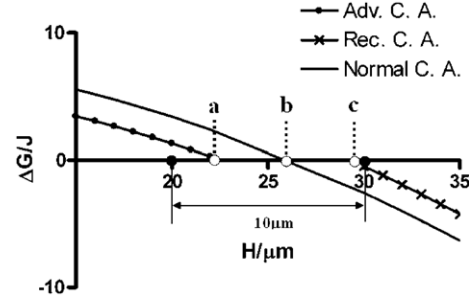


Figure 3. The function of $\Delta G(\theta, H)$ to H while using different values of θ . The pure line is calculated by the normal contact angle, 116.4° , where point b indicates the critical value of H_N when $\Delta G(116.4^\circ, H_N) = 0$. The line with crosses is calculated by the receding contact angle, 107.8° , where point c indicates the critical value of H_U while $\Delta G(107.8^\circ, H_U) = 0$. The line with dots is calculated by the advancing contact angle, 125.8° , where point a indicates the critical value of H_L while $\Delta G(125.8^\circ, H_L) = 0$. Since the displacement of the actuation, $10 \mu\text{m}$, covered the hysteresis region, the actuation is sufficient to switch between the detached and attached modes.

$$G_d = \gamma_{lg} \times (2X + D) + \gamma_{sg} \times D \quad (\text{detach mode}), \quad (4)$$

$$G_a = \gamma_{lg} \times 2\sqrt{(X^2 + H^2)} + \gamma_{sl} \times D \quad (\text{attach mode}), \quad (5)$$

where X is the interval between the higher and lower microposts, D is the diameter of the microposts and H is the difference of the heights between the higher and lower microposts, as illustrated in figure 2(a).

In order to determine the minimum surface energy state, the difference between G_d and G_a is calculated as

$$\begin{aligned} \Delta G(\theta, H) &= G_d - G_a \\ &= \gamma_{lg} \times (2X + D - 2\sqrt{(X^2 + H^2)}) + \gamma_{lg} \times D \times \cos \theta, \end{aligned} \quad (6)$$

where θ represents the water droplet contact angle on a flat hydrophobic surface with a normal value of 116.4° , and X and D are designed to be $80 \mu\text{m}$ and $15 \mu\text{m}$ according to the limitation of the fabrication. The relationship of $\Delta G(\theta, H)$ to H is shown in figure 3. As H is $26.15 \mu\text{m}$ (H_N), ΔG is shown as

$$\Delta G(\theta, H_N) = \Delta G(116.4^\circ, 26.15) = 0. \quad (7)$$

Such a condition means a meta-stable state where the droplet is in either detached or attached mode, as the point b shows in figure 3. Furthermore, as H increases to be larger than $26.15 \mu\text{m}$, the value of ΔG becomes negative and the droplet will be in a detached mode and vice versa. Therefore, the mode switching can be controlled by changing H around the critical value, $26.15 \mu\text{m}$.

However, while considering the contact angle hysteresis, the extra change of H to overcome the hysteresis force needs to be taken into account. When the droplet inclines to be in detached mode, θ will be replaced by the receding contact angle, 107.8° , instead of 116.4° in equation (3). At this moment, the upper limit of H , H_U , that keeps ΔG negative, $\Delta G(107.8^\circ, H_U) \leq 0$, is determined to be $29.35 \mu\text{m}$, as the point c shown in figure 3. Thereby, at an initial state, H is designed to be $30 \mu\text{m}$ which is larger than $29.35 \mu\text{m}$ and leads to $\Delta G(107.8^\circ, 30) = -0.453\gamma_{lg} < 0$; hence, the mode switch from attached to detached can be carried out. In contrast, when the droplet is toward the attached mode, θ will be replaced by the

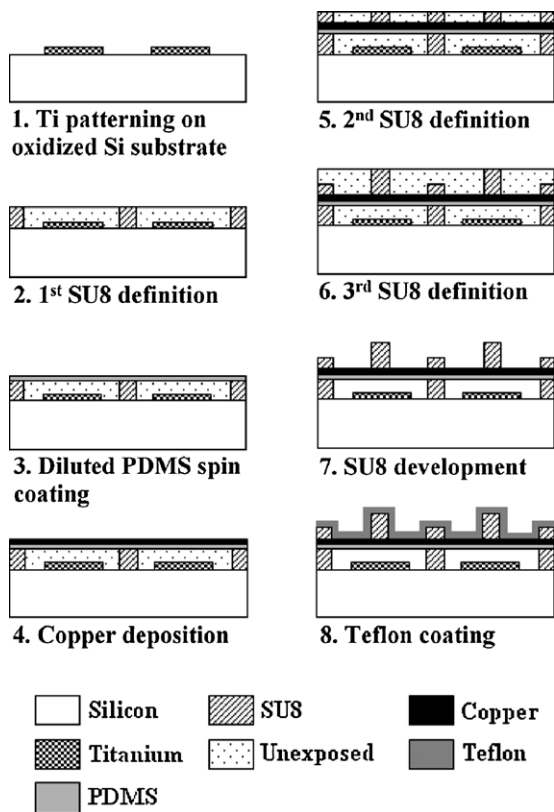


Figure 4. The fabrication process of the SWIM device.

advancing contact angle, 125.8° , in equation (3). The lower limit of H , H_L , is determined as $22.53 \mu\text{m}$, as the point a shown in figure 3. Therefore the sufficient amount of H to keep ΔG being positive is designed as $20 \mu\text{m}$ at the actuation state, and leads to $\Delta G(125.8^\circ, 20) = 1.3\gamma_{lg} > 0$ which can realize the switching from the detached to the attached mode.

Based on the theoretical calculation, the change of H , from $20 \mu\text{m}$ to $30 \mu\text{m}$, can provide enough energy to switch the attached mode to the detached mode under hysteresis resist and vice versa. Therefore, the spacer between the membrane and bottom electrode should be $10 \mu\text{m}$ to satisfy the criterion, and the height of the higher post and the lower post is designed to be $40 \mu\text{m}$ and $10 \mu\text{m}$ respectively. By manipulating the surface between the detached mode and the attached mode, we can reversibly switch the surface wettability through the fraction change of the liquid/solid interface.

4. Fabrication

Major fabrication steps for a SWIM device are illustrated in figure 4. First, the 300 nm titanium layer is deposited on the thermal oxidized silicon substrate by an E-beam evaporator. The titanium layer is patterned by a typical photolithography process and etched by titanium etchant ($\text{NH}_4\text{OH}:\text{H}_2\text{O}_2:\text{H}_2\text{O} = 1:1:2$) (step 1). Then, first negative UV photoresist layer, SU-8, (SU-8 5, MicroChem Corp. USA) was spun coated and exposed without post-exposure bake to allow further reaction with the following polymer material, and its process parameter is adjusted to precisely achieve the designed spacer thickness of $10 \mu\text{m}$ (step 2). Afterward, PDMS liquid is prepared for the

membrane material. In this process, PDMS (Sylgard 184, Dow Corning Corp., USA) and diluent (Fluid 200, Dow Corning Corp., USA) were mixed in a 11:10 weight ratio. This mixture was stirred and degassed thoroughly and then spun coated on the SU-8 resist. Post-baking is exerted to cure PDMS and carry out the cross-linking of SU-8 (step 3), and the minimum thickness of the PDMS membrane achieved is as thin as $3 \mu\text{m}$. Next, the PDMS surface is treated with O_2 plus CF_4 reactive ion etching (RIE) to enhance the adhesion of the following copper film on the PDMS surface. The flow rate of O_2 and CF_4 is controlled at 15 and 5 sccm, respectively [19]. Besides, to avoid overheating to the polymer film, plasma RF power and process time are chosen as 80 W and 60 s, respectively. After the surface treatment is finished, the 120 nm copper deposition is exerted by an E-beam evaporator as soon as possible (step 4). Afterward, the second ($10 \mu\text{m}$) and third ($40 \mu\text{m}$) SU-8 layers were spun coated and exposed (steps 5, 6) to form microposts. The unexposed SU-8 resist is developed by an SU-8 developer (PGMEA, MicroChem Corp., USA) and the free-standing movable metal/polymer membrane is completed (step 7). Finally, 100 nm Teflon (AF1600, DuPont, USA) is spun coated on the surface of the SWIM device (step 8).

In the fabrication process, the most critical step was the fabrication of the copper/PDMS composite membrane. Since the PDMS was fully cross-linked, the low wettability of the PDMS surface would be a barrier for the following metal deposition, and result in failures such as poor adhesion and high residual stress. Typically, metallization of the polymer is performed by etching the polymer surface to increase surface roughness; however, the rough polymer surface also has deleterious effects on the performance of electrical conductivity. Therefore, sufficient adhesion between metal and smooth polymer must be achieved at the same time. Here, we use O_2 plus CF_4 RIE to enhance the adhesion between copper and PDMS. According to the literature [19], the mechanism of formation of functional groups on polymer surfaces by RIE can be interpreted by a two-step model. The first step is the creation of free radicals by surface bombardment. The second step is the formation of functional groups by the interaction between the new radicals and reactive species in the plasma. Comparing to the pure O_2 RIE, the inclusion of CF_4 enables the increase of concentrations of fluorine and fluorine-containing atoms. It is important since the energetic fluorine and fluorine-containing species are more effective in creating polymer radical sites than the oxygen species. As a result, the radical groups generated by the treatment are capable of capturing oxygen to form functional groups on the treated polymer surface. Thus, the O_2 plus CF_4 RIE treatment is well suited to improve the adhesion of the metals to polymers.

On the other hand, the AFM analysis from the literature [19] also showed another shortcoming for pure O_2 RIE. According to the literature [19], if the pure O_2 RIE is exerted, the resulting polymer surface would become much rougher, with a grass-like appearance, than an untreated one. In contrast, the O_2 plus CF_4 RIE treatment is more capable of acquiring a smoother surface. Since the high roughness has the potential to cause detrimental effects on metal covering and metal conductivity, the O_2 plus CF_4 RIE treatment is a more proper choice for our purpose.

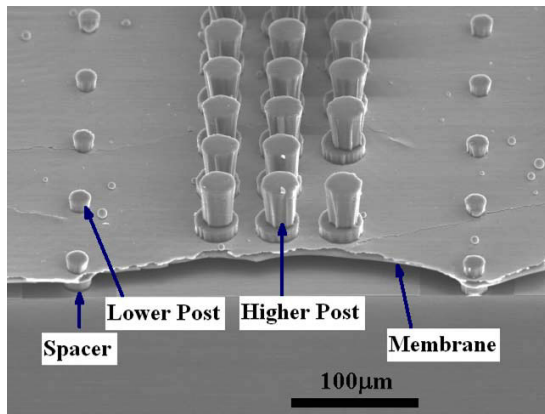


Figure 5. The SEM image of the SWIM device. The higher and lower posts are successively supported by a copper/PDMS composite membrane. The free-standing and flat membrane reveals well-controlled residual stress.

Furthermore, residual stress control in the SWIM device is achieved by adjusting the thickness of the metal layer [20]. For most materials, the less the film thickness is, the more tensile stress is obtained. In contrast, more compressive stress is produced as the film gets thicker. Therefore, in our experiment, we obtained the critical thickness, 120 nm, with almost zero stress. Finally, a functional metal/PDMS interface with sufficient adhesion strength and low residual stress was carried out.

The metal layer can also be used to prevent under-laid SU-8 from exposure. The individual UV definition on each SU-8 layer is able to fabricate the following second and third SU-8 structures. Figure 5 shows the scanning electron microscopic (SEM) pictures of the 3D structures. The cross-section of the

free-standing membrane certified the isolation of a multilayer UV definition and the low residual stress within a metal/PDMS composite membrane. Therefore, the fabrication technique is capable to fabricate complex structures, and showed the potential for various advanced applications.

5. Experiment

To demonstrate the functionality of the device, electric potential was applied to the bottom electrode while the top metal layer was set to ground. In order to achieve sufficient vertical displacement of $10\ \mu\text{m}$, the device was driven in a pull-in mode. Figure 6 shows the results of a pure membrane bending profile measured by an optical interferometer. Figures 6(a) and (b) are the top view of the membrane profile at the initial state and actuated state respectively. Figures 6(c) and (d) are the cross-sections of the membrane bending profile. From the interferometer measurement, at the initial state, the membrane is capable of maintaining flatness. After actuating, figure 6(d) shows that the bending profile consists of inclined planes and a central flat plane, and the central flat plane is in contact with the bottom electrode. Therefore, the result shows that the central flat plane is still able to keep its flatness under actuation. Furthermore, it is evident that the device was driven in a pull-in mode, and the maximum displacement attains the spacer's thickness, $10\ \mu\text{m}$. From the measurement results, the maximum displacement of the membrane fulfills the requirement of minimizing the surface energy mentioned above. Besides, the maximum operation frequency could be achieved with about 20 Hz. It also shows that the response of the actuation is rapid and reversible.

The surface morphology change of the SWIM device is observed by an optical microscope, as shown in figures 7(a)

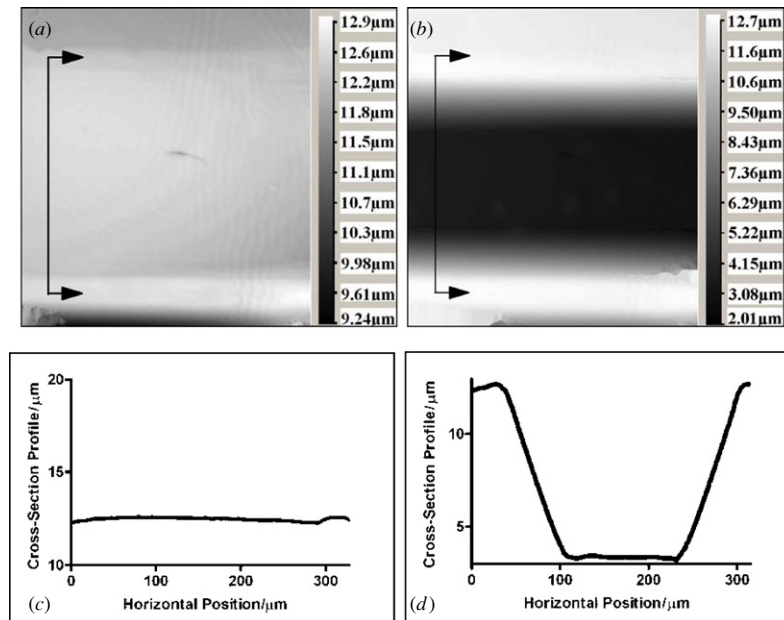


Figure 6. The results of a pure membrane bending profile measured by an optical interferometer. (a) and (b) are the top views of the membrane profile at the initial state and the actuated state, respectively. (c) and (d) are the cross-sections of the membrane bending profile at the initial state and the actuated state, respectively. The results show that the membrane is driven in a pull-in mode, so the maximum displacement is capable of reaching the spacer thickness.

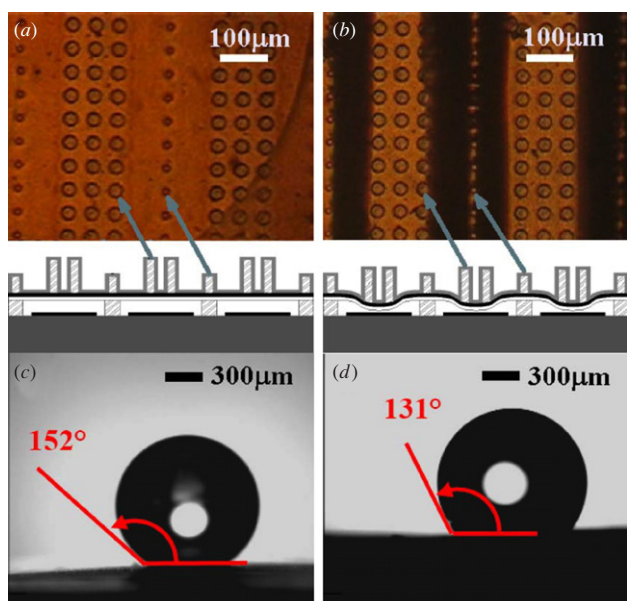


Figure 7. The functionality of SWIM. Before actuation: (a) under optical microscopic observation, the membrane is flat, and (c) the contact angle is 152° . After actuation: (b) under optical microscopic observation, the membrane is bent and the dark areas correspond to the inclined part of the membrane, and (d) the contact angle is 131° .

and (b). Before applying voltage, the membrane with hydrophobic microposts is flat, as illustrated in figure 7(a). As the voltage is applied, the membrane is bent in a pull-in mode, illustrated in figure 7(b). The dark areas shown in figure 7(b) correspond to the inclined part of the membrane, and the area with posts is the part of the membrane that contacts with the bottom electrode. Hence, the images certified that the posts are able to keep themselves being vertical either before or after actuation. The information is important because it shows that the operation of the SWIM device is able to follow the design function.

After switching off the potential, the membrane returns to the initial state as the electrode was discharged, so that the reversibility of surface morphology transformation was obtained. The wettability of the surface is ordinarily represented by the water droplet contact angle measurement, as shown in figures 7(c) and (d). In our experiment, the contact angle measurement is processed by optical image and droplet formation calculation, and the type of water is chosen as $1 \mu\text{l}$ deionized water. At the initial state, the contact angle is 152° , as shown in figure 7(c). After actuation, the contact angle is decreased to 131° by the surface morphology change, as shown in figure 7(d). Apparently, the surface wettability can be changed effectively. Thus, by the theoretical prediction and experiment results, the wettability switching mechanism is certified.

To estimate whether the actuation energy can interfere with bio-molecules in droplets, we conducted experiments to compare the adsorption of bio-molecules on the surfaces of the SWIM device and electrowetting devices. A protein solution of goat anti-rabbit IgG (CHEMICON International, Inc. USA) labeled with fluorescence (Cy5) was employed as the model bio-molecule, at a concentration of 0.1 mg ml^{-1} . The protein solution was dropped on the

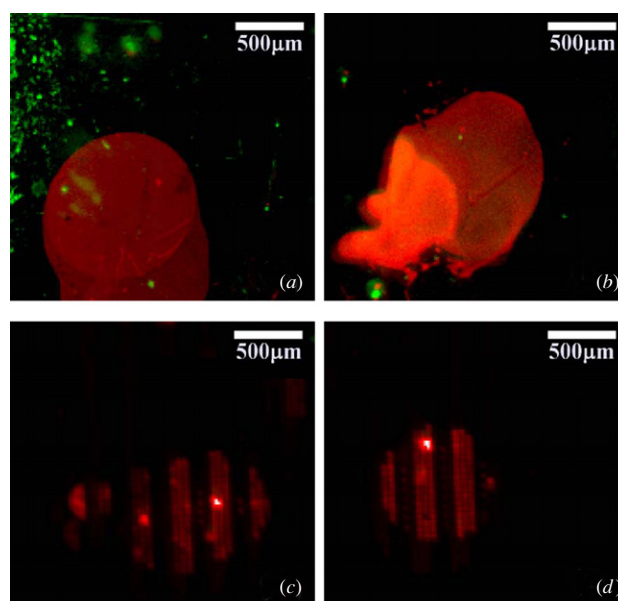


Figure 8. Fluorescence intensity measurement for the absorption of protein on the surface of electrowetting and SWIM devices. (a) The intensity of the electrowetting system before exerting electrical potential, 441 au. (b) The intensity of the electrowetting system after exerting 50 V for 10 minutes, 3031 au. (c) The intensity of the SWIM device before exerting electrical potential, 431 au. (d) The intensity of the SWIM device after exerting 250 V for 10 minutes, 439 au.

SWIM device which was actuated with 250 V and stayed for 10 minutes. An electrowetting device is also employed to demonstrate the effect of an electrical field on the bio-molecules in a droplet. In the electrowetting system, 50 V was applied between the inserted electro probe and bottom planar electrode for 10 minutes. After washing out excess protein solution, the residual proteins on both chip surfaces were visualized by a fluorescence scanner (GenePix 4000B, Axon Instruments, USA) to evaluate the interference of actuation energy on bio-molecules in a droplet. Figures 8(a) and (c) show the fluorescence images of the electrowetting device and the SWIM device before actuation. The fluorescence intensities in figures 8(a) and (b) are at a similar level, 441 au and 431 au, respectively. From the images, the nonspecific absorption of proteins on the Teflon surface of the two devices through either hydrophobic interaction or van der Waals' force is unavoidable. On the other hand, figures 8(b) and (d) show the fluorescence images of both devices after actuation. In the electrowetting system, the mean fluorescent intensity rises up to 3031 au after actuation, which is almost ten times before the actuation, 441 au. The enhancement comes from the attraction of bio-molecules by the penetrated electric field in the droplet. In contrast, the fluorescent intensity on the SWIM device is only 439 au after actuation, which is almost the same due to the confinement of the electric field between the two electrodes. Hence, the shielding mechanism of the SWIM device is verified.

6. Conclusion

We demonstrated a wettability switchable surface driven by an electrostatic-induced surface morphology change (SWIM).

According to the Gibbs free energy and Cassie theory, we designed an electrostatic actuator with microposts of different heights sustained by a copper/PDMS composite polymer membrane for the manipulation of a droplet/surface contact area and contact angle. The device was tested and it was found that the surface wettability could be dynamically switched from superhydrophobic 152° to medium hydrophobic 131° with the application of 250 V. The shielding of the electrical energy on bio-molecules in a droplet is verified in this SWIM device. The wettability switchable surface is suitable to many applications especially in liquid droplet actuation systems for the manipulation of biological reagents.

References

- [1] Cheng Y T, Rodak D E, Wong C A and Hayden C A 2006 Effects of micro- and nano-structures on the self-cleaning behaviour of lotus leaves *Nanotechnology* **17** 1359–62
- [2] Paik P, Pamula V K, Pollack M G and Fair R B 2003 Electrowetting-based droplet mixers for microfluidic systems *Lab Chip* **3** 28–33
- [3] Kuiper S and Hendriks B H W 2004 Variable-focus liquid lens for miniature cameras *Appl. Phys. Lett.* **85** 1128–30
- [4] Farahi R H, Passian A, Ferrell T L and Thundat T 2004 Microfluidic manipulation via Marangoni forces *Appl. Phys. Lett.* **85** 4237–9
- [5] Sun T, Wang G, Feng L, Liu B, Ma Y, Jiang L and Zhu D 2004 Reversible switching between superhydrophilicity and superhydrophobicity *Angew. Chem. Int. Ed.* **43** 357–60
- [6] Lahann J, Mitragotri S, Tran T-N, Kaido H, Sundaram J, Choi I S, Hoffer S, Somorjai G A and Langer R 2003 A reversibly switching surface *Science* **299** 371–4
- [7] Welters W J J and Fokkink L G J 1998 Fast electrically switchable capillary effects *Langmuir* **14** 1535–8
- [8] Pollack M G, Fair R B and Shenderov A D 2000 Electrowetting-based actuation of liquid droplets for microfluidic applications *Appl. Phys. Lett.* **77** 1725–6
- [9] Brinkmann M and Lipowsky R 2002 Wetting morphologies on substrates with striped surface domains *J. Appl. Phys.* **92** 4296–306
- [10] Ichimura K, Oh S-K and Nakagawa M 2000 Light-driven motion of liquids on a photoresponsive surface *Science* **288** 1624–6
- [11] Xu L, Chen W, Mulchandani A and Yan Y 2005 Reversible conversion of conducting polymer films from superhydrophobic to superhydrophilic *Angew. Chem. Int. Ed.* **44** 6009–12
- [12] Wang X, Ederth T and Inganäs O 2006 In situ Wilhelmy balance surface energy determination of poly(3-hexylthiophene) and poly(3,4-ethylenedioxythiophene) during electrochemical doping-dedoping *Langmuir* **22** 9287–94
- [13] Lee J, He B and Patankar N A 2005 A roughness-based wettability switching membrane device for hydrophobic surfaces *J. Micromech. Microeng.* **15** 591–600
- [14] Yoon J-Y and Garrell R L 2003 Preventing biomolecular adsorption in electrowetting-based biofluidic chips *Anal. Chem.* **75** 5097–102
- [15] Feng L, Li S, Li Y, Li H, Zhang L, Zhai J, Song Y, Liu B, Jiang L and Zhu D 2002 Super-hydrophobic surfaces: from natural to artificial *Adv. Mater.* **14** 1857–60
- [16] Krupenkin T N, Taylor J A, Schneider T M and Yang S 2004 From rolling ball to complete wetting: the dynamic tuning of liquids on nanostructured surfaces *Langmuir (Letter)* **20** 3824–7
- [17] Cassie A B D and Baxter S 1944 Wettability of porous surfaces *Trans. Faraday Soc.* **40** 546
- [18] Adamson A W 1982 *Physical Chemistry of Surfaces* (New York: Wiley)
- [19] Ge J and Kivilahti J K 2002 Effects of surface treatments on the adhesion of Cu and Cr/Cu metallizations to a multifunctional photoresist *J. Appl. Phys.* **92** 3007–15
- [20] Ennos A E 1966 Stresses developed in optical film coatings *Appl. Opt.* **5** 51–62